Modeling the global ocean iron cycle

Payal Parekh,[1] Michael J. Follows, and Edward Boyle

Department of Earth, Atmosphere and Planetary Sciences, Massachusetts Institute of Technology, Cambridge, Massachusetts, USA

Received 5 March 2003; revised 20 June 2003; accepted 15 August 2003; published 7 January 2004.

[1] We describe a model of the ocean transport and biogeochemical cycling of iron and the subsequent control on export production and macronutrient distributions. Ocean transport of phosphorus and iron are represented by a highly idealized six-box ocean model. Export production is parameterized simply; it is limited by light, phosphate, and iron availability in the surface ocean. We prescribe the regional variations in aeolian deposition of iron and examine three parameterizations of iron cycling in the deep ocean: (1) net scavenging onto particles, the simplest model; (2) scavenging and desorption of iron to and from particles, analogous to thorium; and (3) complexation. Provided that some unknown parameter values can be set appropriately, all three biogeochemical models are capable of reproducing the broad features of the iron distribution observed in the modern ocean and explicitly lead to regions of elevated surface phosphate, particularly in the Southern Ocean. We compare the sensitivity of Southern Ocean surface macronutrient concentration to increased aeolian dust supply for each parameterization. Both scavenging-based representations respond to increasing dust supply with a drawdown of surface phosphate in an almost linear relationship. The complexation parameterization, however, asymptotes toward a limited drawdown of phosphate under the assumption that ligand production does not respond to increased dust flux. In the scavenging based models, deep water iron concentrations and, therefore, upwelled iron continually increase with greater dust supply. In contrast, the availability of complexing ligand provides an upper limit for the deep water iron concentration in the latter model. *INDEX TERMS:* 4805 Oceanography: Biological and Chemical: Biogeochemical cycles (1615); 4842 Oceanography: Biological and Chemical: Modeling; 4845 Oceanography: Biological and Chemical: Nutrients and nutrient cycling; 4875 Oceanography: Biological and Chemical: Trace elements; *KEYWORDS:* modeling, ocean iron cycle

Citation: Parekh, P., M. J. Follows, and E. Boyle (2004), Modeling the global ocean iron cycle, *Global Biogeochem. Cycles*, *18*, GB1002, doi:10.1029/2003GB002061.

1. Introduction

[2] Fertilization experiments have shown iron (Fe) to be a limiting nutrient of primary production in "high nutrient, low chlorophyll" regions of the oceans such as the Southern Ocean, the northern North Pacific, and the equatorial Pacific [*Martin et al.*, 1994; *Coale et al.*, 1996; *Boyd et al.*, 2000]. Reflecting iron's role in the biological cycle, its vertical profile is nutrient-like with low concentrations at the surface due to biological uptake, and higher concentrations at depth due to remineralization of biogenic matter. Owing to the analytical difficulty of measuring iron, the deep water iron distribution is currently poorly resolved, but it is clear that large-scale, deep water Fe gradients do not mirror those of nitrate and phosphate. Rather, concentrations are highest in the Atlantic (0.6–0.8 n*M*), intermediate in the Indo-Pacific basin (0.4–0.7 n*M*), and lowest in the Southern Ocean (0.2–0.3 n*M*) (Figure 1). This reflects the regional patterns of the aeolian source, physical transport, and the water column cycling of iron.

1.1. Biogeochemistry of Iron in the Oceans

[3] Like other metals, such as lead and aluminum, iron has an episodic aeolian source to the surface ocean, and it is removed from the water column by scavenging onto sinking particles. Direct quantitative estimates of scavenging rates of Fe have not yet been made, though *Bruland et al.* [1994] indirectly estimate a residence time for Fe between 70 and 140 years in the water column. Thorium (Th) is a metal that has similar abiological properties to Fe. *Bacon and Anderson* [1982] calculate an oceanic scavenging rate for Th and also suggest that scavenged Th is released back to the water column. They describe the latter process as a first-order reaction proportional to the particulate Th concentration, estimating redissolution rates of 1.33–6.30 yr^{-1}. Since Fe and Th have similar metallic properties, it seems reasonable to speculate that scavenged Fe on particles may also

[1] Also at Department of Marine Chemistry and Geochemistry, Woods Hole Oceanographic Institution, Woods Hole, Massachusetts, USA.

0886-6236/04/2003GB002061$12.00

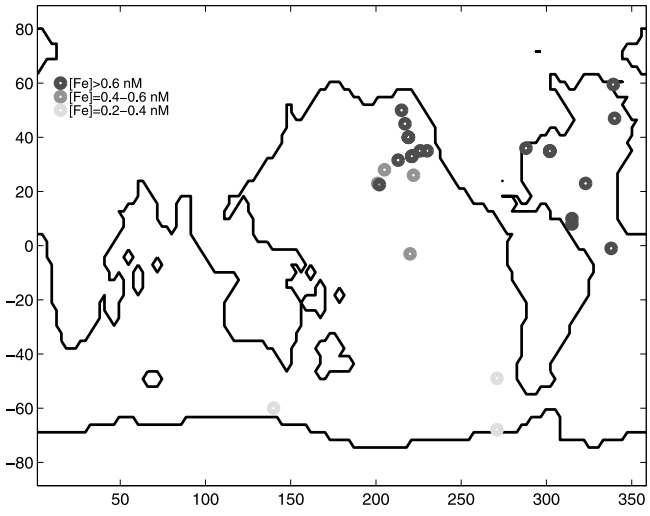

Figure 1. Observed dissolved [Fe] (<0.4 μm) at 1000 m. Data sources: *Bell et al.* [2002], E. Boyle (unpublished data), *Bruland et al.* [1994], *de Baar et al.* [1999], *Johnson et al.* [1997, and references therein], *Powell and Donat* [2001], *Rue and Bruland* [1995], *Sohrin et al.* [2000], *Wu and Luther* [1994], *Wu et al.* [2001], and *Wu and Boyle* [2002]. See color version of this figure at back of this issue.

be subject to redissolution. Naturally, the rate of Fe desorption may vary significantly from that of Th desorption.

[4] Studies suggest that 99% of dissolved iron (i.e., that which passes through a 0.4 μm filter) is bound to organic ligands throughout the world's oceans [*Gledhill and van den Berg*, 1994; *Rue and Bruland*, 1995; *van den Berg*, 1995; *Wu and Luther*, 1995; *Rue and Bruland*, 1997; *Gledhill et al.*, 1998; *Nolting et al.*, 1998; *Witter and Luther*, 1998; *Witter et al.*, 2000; *Boye et al.*, 2001; *Powell and Donat*, 2001]. Estimates of the concentration of ligand range between 0.5 and 6 n*M*. Vertical ligand profiles appear nutrient-like with ligand concentration below 1000 m remaining relatively constant. The estimated conditional stability constant of the ligand(s) (K_{FeL}) ranges between $10^{9.8} M^{-1}$ and $10^{14.3} M^{-1}$ without any clear regional pattern. Most studies suggest only one class of active organic ligand, but two studies [*Rue and Bruland*, 1997; *Nolting et al.*, 1998] have inferred two ligand classes, in the North Pacific and the Pacific sector of the Southern Ocean. The source and chemical characterization of the ligands are unknown, but *Macrellis et al.* [2001] have been able to extract iron-binding compounds from seawater and characterize certain functional groups (i.e., site of chemical reactivity in a molecule) within the compound. They found that functional groups known to be present in marine and terrestrial siderophores are present in the marine environment, suggesting that the ligands are produced biologically by phytoplankton to aid in the uptake of Fe from seawater.

1.2. Prior Modeling Studies

[5] *Bruland et al.* [1994] and *Boyle* [1997] suggested that the variable aeolian input into each ocean basin coupled with the biological processes of uptake/regeneration and the metallic property of scavenging could explain the profile of Fe in the world's oceans. *Johnson et al.* [1997] suggest that iron's complexation to an organic ligand must be controlling the deep water distribution.

[6] *Lefévre and Watson* [1999] and *Archer and Johnson* [2000] developed models to examine possible controls on deep water Fe gradients. *Lefévre and Watson* [1999] use a 10-box representation of the ocean adapted from the PANDORA model [*Broecker and Peng*, 1986, 1987], parameterizing scavenging of iron onto particles, as well as its biological consumption, remineralization, and aeolian deposition. With a scavenging rate of 0.005 yr^{-1} and solubility of the aeolian iron supply of 2%, their model was able to reproduce the broad features of the deep water iron gradients (as observed today), although the absolute concentrations are high in the deep Atlantic (1.6 n*M*). *Lefévre and Watson* [1999] also introduced a parameterization of complexation and scavenging, which assumed an effective solubility of iron (Fe_{sol}) to represent the iron complexed by a ligand, having a uniform oceanic concentration of 0.6 n*M*. Iron loss was parameterized as a damping toward the effective solubility, $-k \times ([Fe] - Fe_{sol})$, with a timescale of $1/k = 100$ years, assuming that only iron which exceeds the effective solubility (i.e., is not bound to the ligand) can be scavenged from the water column. Implicitly, complexation to the ligand is assumed to be very rapid. In this model, deep water concentrations in the Antarctic and the Indo-Pacific were approximately 0.6 n*M*, and the deep Atlantic is somewhat higher with a concentration of 0.92 n*M*. The concentrations are higher than currently observed in the Atlantic and Indo-Pacific. However, at the time of that study, this model seemed more consistent with the available evidence, which was interpreted to show that the deep water iron concentration was uniform in all basins. There were no measurements from the Southern Ocean at that time.

[7] *Archer and Johnson* [2000], using a three-dimensional, global circulation and biogeochemistry model, examine three parameterizations of iron cycling: (1) scavenging only, (2) complexation with one ligand, and (3) complexation with two (strong and weak) ligands. In the first case, using a slow scavenging rate (1.6×10^{-3} yr^{-1}), the deep water distribution reflects that of a typical nutrient. In the second case, representing complexation with a very strong ligand ($K = 1.2 \times 10^{13}$) of uniform concentration (0.6 n*M*) results in a uniform deep water Fe distribution, consistent with the observations and their interpretation at the time. In the third case, *Archer and Johnson* [2000] apply the profile of two iron-binding ligands, a strong ligand ($K = 1.2 \times 10^{13} M^{-1}$) in the upper 500 m with a maximum concentration of 0.5 n*M* and a weaker ligand ($K = 3 \times 10^{11} M^{-1}$) with concentrations ranging between 1.5 and 2.5 n*M* from the surface to depth, as measured by *Rue and Bruland* [1995] in the North Pacific. This model simulation results in roughly equal deep water [Fe] in the Atlantic and Pacific basins. In this scenario, excess iron at the surface not utilized biologically was removed from the system, representing an unidentified process.

[8] There is particular interest in the role of iron and aeolian dust supply in the modulation of the surface nutrient concentration of the Southern Ocean and the ocean's

biological pumps of carbon [*Martin*, 1990]. There is evidence from ice cores [*Petit et al.*, 1999] and suggestions from numerical models [*Mahowald et al.*, 1999] indicate an increased aeolian supply of iron throughout the oceans during periods of glaciation. Numerical ocean models have been used to explore the implications for the carbon cycle by examining the response to imposed surface nutrient drawdown [e.g., *Sarmiento and Orr*, 1991]. *Watson et al.* [2000] used a simplified ocean biogeochemistry model with explicit representation of iron cycling, forced with glacial-interglacial cycles in Southern Ocean iron deposition derived from ice core dust records. Their study suggests that a significant fraction of the observed glacial-interglacial change in atmospheric CO_2 may be accounted for in this way. Deep water iron cycling is represented in that model as a particulate scavenging process. In contrast, *Leféevre and Watson* [1999] found it necessary to increase dust flux globally by a factor of 10 in order to drawdown modeled pCO_2 50 μatm. *Archer and Johnson* [2000] examine the response of surface phosphate loading to increased aeolian dust supply in their global, three-dimensional model in which deep ocean iron cycling is represented as a combination of complexation to organic ligands and scavenging by particles. They show that a significant drawdown of the surface macro-nutrients can be achieved with high ligand concentrations.

1.3. Aims of This Study

[9] New data from the Pacific and Southern Oceans [*de Baar et al.*, 1999; *Powell and Donat*, 2001; *Sohrin et al.*, 2000; *Wu et al.*, 2001; E. Boyle et al., Iron, manganese, and lead at Hawaii Ocean Time-series Station ALOHA: Temporal variability and an intermediate water hydrothermal plume, submitted to *Geochimica Cosmochimica Acta*, 2003] show the distribution of dissolved iron in the deep ocean differs significantly from the uniformity that the models of *Leféevre and Watson* [1999] and *Archer and Johnson* [2000] sought to reproduce and understand. Concentrations now appear to be lowest in the Southern Ocean and highest in the Atlantic basin. In the Pacific, [Fe] appears to have highest concentrations in the North Pacific (0.6 n*M*), but decreases in the subtropical and tropical Pacific (0.4–0.5 n*M*) (Figure 1). These models and parameterizations need to be revisited in the light of the new data.

[10] In addition, recent measurements indicate a range in the strength of the conditional stability constant and the presence of a significant amount of free ligand. The *Leféevre and Watson* [1999] model does not account for these observations. *Archer and Johnson*'s [2000] model adds a weaker ligand in their two-ligand scenario, but still has a strong ligand at the surface, which requires the bioavailability of Fe reaching the high latitudes to be reduced relative to the rest of the model domain to keep surface $[PO_4]$ high in the high-latitude surface waters.

[11] Here we aim to build on these previous studies and use more recent data to adapt and constrain the parameterizations of iron cycling in the deep oceans. We will also explore the implications for our understanding of the global nutrient and carbon cycle. In order to allow significant exploration of parameter space, we use a computationally economical, though highly idealized, six-box model of ocean biogeochemistry similar to that of *Leféevre and Watson* [1999] and *Broecker and Peng* [1986, 1987]. We test three parameterizations of iron cycling with the model: (Case I) net scavenging onto particles, (Case II) explicit representation of scavenging and desorption to and from particles, and (Case III) complexation. We will show that, provided appropriate parameter values are chosen, each of these parameterizations can reproduce the broad characteristics of the presently observed deep ocean dissolved iron distribution. However, only the third case concurrently reproduces the observed deep water gradients and the speciation of iron and ligand. We will also demonstrate that the response of surface phosphate to increasing dust supply is very sensitive to whether ocean iron is controlled by scavenging and desorption or complexation.

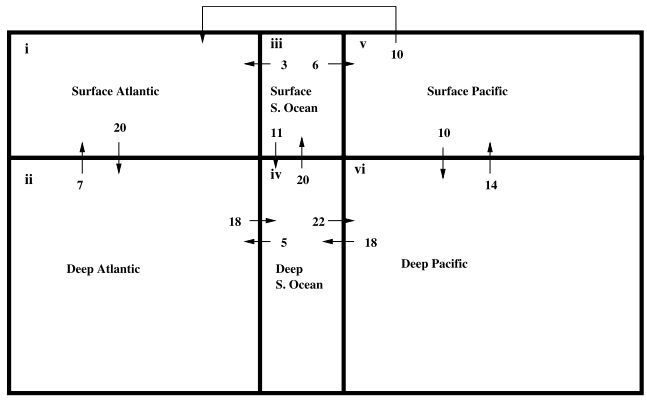

Figure 2. Schematic diagram of box model adapted from *Broecker and Peng* [1986, 1987]. The arrows represent volume transport (Sv).

[12] In the following sections we will outline the structure and mechanics of the six-box ocean biogeochemistry model, discuss model results and sensitivities for each of the three iron parameterizations outlined above, and assess the sensitivity to increased aeolian supply and decreased overturning in the Southern Ocean for each parameterization. Finally, we will discuss the implications of these models for modeling studies including prognostic, three-dimensional models of ocean circulation and biogeochemistry.

2. Global Ocean Biogeochemistry Model

[13] We use a six-box model (Figure 2) similar in construction to *Broecker and Peng*'s [1986, 1987] PANDORA Model, representing the surface and deep waters of the Atlantic, Antarctic, and Indo-Pacific basins. Each basin is divided into two layers, a 100-m surface layer where biological uptake of nutrients occurs, and a deep layer. *Broecker and Peng* [1987] tuned volume transports to optimize the modeled ^{14}C distribution. We recognize that such highly idealized models have limitations, particularly for quantitative assessments [*Broecker et al.*, 1999; *Archer et al.*, 2000; *Follows et al.*, 2002], but they do provide a useful framework in which to develop clear, qualitative understanding and preliminary sensitivity studies. The model is

solved numerically using a time step of 2.5 days and is integrated until steady state is reached. The solution is assumed to reach steady state when the tendency changes by less than 0.2% over 50 years.

2.1. Representation of Macro-Nutrient Cycling

[14] The tracers explicitly carried in our model are phosphate (PO_4), dissolved organic phosphorus (DOP), total dissolved iron (Fe_T), and particulate inorganic iron (Fe_P). Biological uptake and regeneration is indexed to phosphorus. We illustrate the mechanics of the model's phosphorus cycle with the prognostic equations for phosphate (PO_4) and dissolved organic phosphate (DOP) for the surface and deep Atlantic (boxes i and ii in Figure 2). For the surface,

$$\frac{dPO_4^i}{dt} = -u \cdot \nabla PO_4^i - \Gamma + \lambda DOP^i, \quad (1)$$

$$\frac{dDOP^i}{dt} = -u \cdot \nabla DOP^i - \Gamma f_{DOP^i} - \lambda DOP^i, \quad (2)$$

$$\Gamma = \mu PO_4^i \frac{Fe_T^i}{Fe_T^i + K_s}. \quad (3)$$

[15] Superscript numerals indicate the relevant model reservoir. The first term on the right-hand of equation (1) indicates transport by the model's circulation, the second represents new production, and the third term represents the remineralization of DOP. Biological uptake and export are limited by light, phosphate, and iron (equation (3)). In conditions where Fe and light are replete, we assume surface PO_4 to be the limiting nutrient which is exported with a characteristic timescale, $1/\mu$ of about 1 month. Iron limitation is represented by Michaelis-Menten kinetics. The half-saturation constant (K_s) is globally uniform but is adjusted, within the range of measured values [*Price et al.*, 1994; *Fitzwater et al.*, 1996] to optimize the modeled surface [PO_4] and [Fe_T] distributions. For the deep,

$$\frac{dPO_4^{ii}}{dt} = -u \cdot \nabla PO_4^{ii} + \Gamma(1 - f_{DOP^i}) + \lambda DOP^{ii} \quad (4)$$

$$\frac{dDOP^{ii}}{dt} = -u \cdot \nabla DOP^{ii} - \lambda DOP^{ii}. \quad (5)$$

[16] In equation (4), the first term on the right-hand side represents transport, the second represents the remineralization of sinking particulate matter, and the third represents the remineralization of DOP.

[17] Two thirds of new production (f_{DOP}) enters the surface dissolved organic phosphorus (DOP) pool, while one third is rapidly exported as particulate to the deep PO_4 pool [*Yamanaka and Tajika*, 1997]. The imposed timescale for remineralization of DOP, ($1/\lambda$), is 6 months.

Table 1. Aeolian Fe Dust Data (g Fe yr^{-1})[a]

Basin	Gao	Duce/Tindale	Jickell/Spokes	Model Values
Atlantic	7.73	8.54	6.46	6.46
Southern Ocean	0.071	–	–	0.071
Indo-Pacific	5.71	23.5	10.17	10.17

[a]Data sets included are those of *Duce and Tindale* [1991], *Gao et al.* [2001], and *Jickells and Spokes* [2002].

Table 2. Model Parameters

Symbol	Definition	Value
R_{Fe}	Fe:C ratio	25 μmol:1mol
f_{DOP}	fraction of DOP	0.67
h	depth of surface box	100 m
H	depth of deep box	3900 m
F_{in}	aeolian deposition rate	see Table 1
α	Fe dust solubility	1%
μ	biological uptake rate	1 $month^{-1}$
λ	remineralization rate	0.5 yr^{-1}
k_{sc}	scavenging rate	variable
k_b	desorption rate	variable
W_s	particle sinking velocity	2900 m yr^{-1}
K_s	iron half saturation constant	0.2 nM
K_{FeL}	ligand conditional stability constant	variable

2.2. Iron Cycling

[18] The aeolian source of iron is prescribed, while the loss of iron due to scavenging, as well as iron's role in the biological cycle, are modeled explicitly. Total dissolved iron (Fe_T) and particulate inorganic iron (Fe_P) are prognostic tracers of the model. The following equations describe the iron cycle for the surface and deep Atlantic (boxes i and ii in Figure 2) for the surface. The equations for the other basins are similar. For the surface,

$$\frac{dFe_T^i}{dt} = \alpha F_{in} - u \cdot \nabla Fe_T^i - \Gamma R_{Fe} + \lambda DOP^i R_{Fe} + J_{Fe}^i \quad (6)$$

$$\frac{dFe_P^i}{dt} = -J_{Fe}^i - Ws \frac{\partial}{\partial z} Fe_P^i. \quad (7)$$

[19] The first term on the right-hand side in equation (6) represents the aeolian source, the second term represents ocean transport of total iron, and the third term represents biological utilization. Remineralization of DOM is represented by the fourth term on the right-hand side, and the fifth, J_{Fe}^i, represents the interactions with particles or ligands which differs between each of the three parameterizations and will be described in more detail below.

[20] Aeolian deposition (F_{in}) is the source of iron to the model ocean. Iron deposition data from *Gao et al.* [2001], *Duce and Tindale* [1991], and *Jickells and Spokes* [2002 and references therein] were used to estimate the source to the surface waters of each basin. Table 1 summarizes the various data sets and the values used. The solubility of Fe aerosols (α) in seawater is not well known, although recent studies suggest it may be below 5% [*Spokes and Jickells*, 1996; *Jickells and Spokes*, 2002 and references therein]. On the basis of results of parameter space exploration, we use $\alpha = 0.01$ (i.e., 1% solubility) for the models discussed here (Table 2).

[21] Iron is biologically utilized in proportion to PO_4 with a fixed Fe:C ratio (R_{Fe}) and a C:P Redfield ratio of 106:1.

Table 3. Modeled Surface and Deep [PO_4] for "Best-Fit" Scenario for Each Case[a]

Basin	Observed	Case I	Case II	Case III
Surface Atlantic	0.45	0.35	0.38	0.40
Surface Southern Ocean	01.74	1.7	1.7	1.7
Surface Indo-Pacific	0.51	0.83	0.85	0.79
Deep Atlantic	1.56	1.3	1.4	1.5
Deep Southern Ocean	2.24	1.8	1.8	1.9
Deep Indo-Pacific	2.42	2.3	2.3	2.2
Global average	2.17	2	2	2

[a]In case I, $k_{sc} = 0.004$ yr^{-1}. For case II, $k_{sc} = 0.04$ yr^{-1}, $k_b = 6$ yr^{-1}. For case III, $k_{sc} = 0.19$ yr^{-1}, $\log(K_{Fel}) = 11$. Units are in μM. Average observed value for each basin is taken from *Conkright et al.* [2002].

Sunda and Huntsman [1995] have published estimates for the Fe:C ratio that indicate marine phytoplankton decrease their cellular iron requirement to optimize growth in Fe-stressed environments but we have not represented this variability here, as a clear relationship has not been established. The Fe:C ratio is equal to 25 μmol:1mol to optimize surface [PO_4]. The half-saturation constant (K_s) equals 0.2 nM.

[22] Evidence from Th isotopes indicates that the mean sinking rates of fine particles is between 500 and 1000 myr^{-1} [*Cochran et al.*, 1993]. In order to very crudely account for the different sinking rates of large and small particles, we have assumed that 10% of particles are large with a sinking rate of 20,000 myr^{-1} and 90% are small particles with a sinking rate of 1000 myr^{-1}, yielding an average sinking rate (W_s) of 2900 myr^{-1}.

[23] The deep equations for iron are

$$\frac{dFe_T^{ii}}{dt} = -u \cdot \nabla Fe_T^{ii} + \Gamma R_{Fe}(1 - f_{DOP})R_{Fe} + J_{Fe}^{ii} \quad (8)$$

$$\frac{dFe_P^{ii}}{dt} = -J_{Fe}^{ii} - Ws\frac{\partial}{\partial z}Fe_P. \quad (9)$$

[24] We examine three different parameterizations for the geochemical processes: (Case I) net scavenging, (Case II) desorption, and (Case III) complexation. In the first and second cases, we do not differentiate between complexed and free iron and assume that the total iron pool is subjected to all geochemical processes. In the third case, we explicitly model complexation and differentiate between free iron and complexed iron.

3. Model Results

[25] While we will focus on the iron distribution in this discussion, the phosphate distribution, which is explicitly controlled by iron limitation here, also provides a consistency check on the model. For solutions when iron distribution is reasonable, the phosphate distributions are in good agreement with observations.

[26] Surface [PO_4] is elevated in the Southern Ocean box, depleted in the Atlantic box, and intermediate in the Indo-Pacific box. Deep PO_4 increases from the Atlantic to the Indo-Pacific. Table 3 summarizes modeled surface and deep [PO_4] for the "best-fit" scenario for each case. For reference, averaged [PO_4] from *Conkright et al.* [2002] are also shown. While the focus of this study is on deep water Fe gradients, surface [Fe_T] are calculated also. Surface [Fe_T] is essentially depleted in each surface basin.

3.1. Case I: Net Scavenging Model

[27] *Boyle* [1997] suggested that the deep water distribution of iron may be modeled using simple parameterizations of aeolian deposition, biological uptake and remineralization of organic matter, and a representation of net scavenging to particles. Such a model is highly idealized, and does not attempt to explicitly represent the details of the biogeochemical processes, but it could be the simplest viable prognostic model for iron in the ocean. It has only one adjustable parameter and does not attempt to describe poorly understood details of the biogeochemical processes.

[28] Here we examine whether this parameterization can reproduce the broad basin to basin and surface to deep ocean observed gradients of dissolved iron. Specifically, we look for a solution where average deep water concentrations are highest in the Atlantic (0.6 nM), intermediate in the Indo-Pacific basin (0.4–0.5 nM), and lowest in the Southern Ocean (0.3 nM). In this formulation, Fe_T is scavenged and is utilized biologically. This parameterization is conceptually similar to the no-ligand model of *Lefèvre and Watson* [1999]. We impose the regional variations in aeolian supply and examine the sensitivity of the dissolved iron distribution to the net scavenging rate. In this case the loss of iron is modeled simply as a first-order scavenging process, limited by the dissolved free Fe concentration. Scavenged iron is transferred to the particulate pool, Fe_p, with rate constant $-k_{netsc}$, and is stripped from the water column as the particles sink. Here, then,

$$J_{Fe} = -k_{netsc}Fe_T. \quad (10)$$

[29] Figure 3 shows the deep ocean, dissolved iron concentrations in each of the three modeled regions

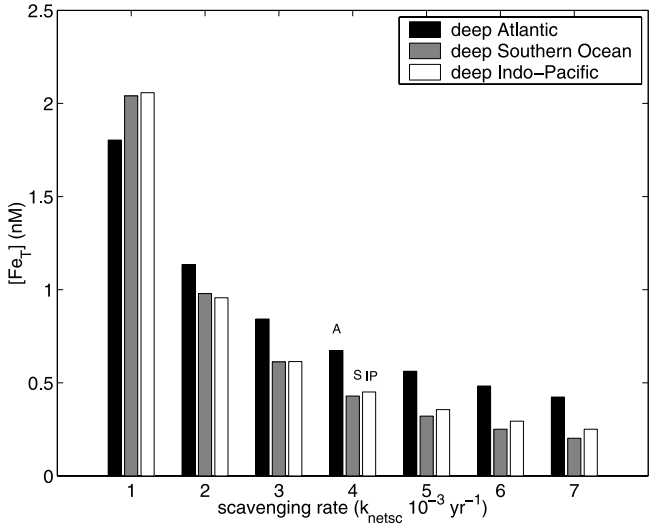

Figure 3. Sensitivity of deep [Fe_T] to scavenging rates. For slow scavenging rates, ($k_{netsc} < 0.001$), the Fe_T distribution is nutrient-like. For intermediate scavenging rates, $0.004 < k_{netsc} < 0.006$, the observed gradients are reproduced. For $k_{netsc} > 0.006$, the sense of gradient is reproduced, although mean concentrations are lower than observed.

(Atlantic basin, Southern Ocean, Pacific basin) as a function of the net scavenging rate. Each cluster of three bars represents the solution of the model at a particular value of scavenging rate. The relative lengths of the three bars reflect the basin to basin gradients of deep iron in each solution. In the case of a slow net scavenging rate (k_{netsc} = 0.001 yr^{-1}), the deep water distribution is that of a typical nutrient with the deep Indo-Pacific iron concentration greater than the deep Southern Ocean which is greater than the deep Atlantic. The result is unsurprising, but the gradients are not as observed. For stronger scavenging, k_{netsc} > 0.004 yr^{-1}, the observed deep water Fe gradients (Atl > Indo-Pacific > Southern Ocean) are reproduced. However, when k_{netsc} > 0.006 yr^{-1}, though the inter-basin gradients remain of the correct sign, the mean ocean deep water [Fe] becomes considerably too low.

[30] This simple model, representing the basin variations of the aeolian supply and a uniform, net scavenging rate can reproduce the unique deep water iron signature provided that 0.004 yr^{-1} < k_{sc} < 0.006 yr^{-1}. This is consistent with the previous study of *Leféyre and Watson* [1999].

3.2. Case II: Scavenging-Desorption Model

[31] While the highly simplified model of Case I can reproduce the broad, basin to basin gradients of the dissolved iron distribution, it does not resolve the biogeochemical processes at work. In Cases II and III, we introduce more detailed parameterizations which attempt to represent processes known to be, or likely to be, at work in the ocean. We ask if these more detailed models can reproduce the observations and, if so, what constraints can be placed on system parameters by the observations?

[32] Thorium is produced in the ocean by radio decay and is subsequently scavenged out of the water column by sinking particles. *Bacon and Anderson* [1982], using oceanic observations of thorium isotopes, have estimated a scavenging (absorption) rate between 0.2 and 1.28 yr^{-1} and a net scavenging rate of ~30 years. This is much faster than the net scavenging rate for iron implied in our model (Case I). *Bacon and Anderson* [1982] suggest that scavenged Th is also desorbed from particles, i.e., released back to the water column, and also infer from data a rate at which this occurs. Since Fe and Th have similar metallic properties, we consider it likely that iron may experience a similar dynamic interplay of scavenging and desorption to and from particles.

[33] To address this possibility in Case II, we parameterize the interactions of iron with particles in the deep water as a cycle of rapid scavenging and desorption which may result in a slow net scavenging consistent with the observed distribution and Case I above (Figure 4). In this case,

$$J_{Fe} = -k_{sc} Fe_T + k_b Fe_P. \quad (11)$$

Here $-k_{sc}$ is the scavenging rate. Scavenging is proportional to the availability of dissolved iron; k_b is the desorption rate, and desorption is proportional to particulate iron. Figure 5 shows the deep water, dissolved iron concentration in each of the model regions as a function of scavenging rates

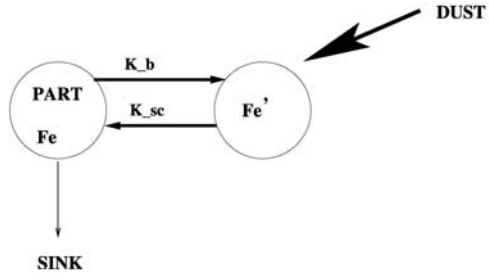

Figure 4. Schematic description of the scavenging and desorption model. Desorption is treated as a first-order process dependent on the particulate iron concentration and transfers particulate Fe to the dissolved pool. Scavenging is modeled as a first-order process dependent on the dissolved Fe concentration. Scavenged iron can be lost from the ocean, ultimately balancing the aeolian sink.

ranging between 0.1 and 1 yr^{-1} and desorption rates between 20 and 100 yr^{-1}. When the ratio of desorption/scavenging is ~150–170, this model is able to broadly reproduce the observed global deep water Fe gradients and concentrations (dashed contours).

[34] For thorium, the desorption to scavenging ratio is calculated to be an order of magnitude smaller. We might interpret these model results to suggest that iron and thorium may behave in a similar manner, but have different desorption to scavenging ratios. On the other hand, there are other processes which may be significant for iron and which we should include in the model.

3.3. Case III: Complexation

[35] Case II again found a plausible solution of the model by representing iron as an analogue of thorium, provided appropriate scavenging and desorption rates are applied. New methods and observations of iron in the ocean would be required to directly confirm such a mechanism at work. However, there is a great deal of evidence that another biogeochemical process, complexation with organic ligands, plays a significant role in the control of deep water iron distributions.

[36] Observational evidence [*Gledhill and van den Berg*, 1994; *Rue and Bruland*, 1995; *van den Berg*, 1995; *Wu and Luther*, 1995; *Rue and Bruland*, 1997; *Gledhill et al.*, 1998; *Nolting et al.*, 1998; *Witter and Luther*, 1998; *Witter et al.*, 2000; *Boye et al.*, 2001; *Powell and Donat*, 2001] indicates that over 99% of "dissolved" iron is bound to a ligand. In this third case we add a mechanistic description of Fe complexation to our box model (Figure 6). Representations of the effect of complexation have been introduced in two previous models (see section 1). The model applied here is closely related to the (second) model of *Archer and Johnson* [2000] representing complexation with a single ligand imposing [L_T]. In the *Archer and Johnson* [2000] model, L_T = 0.6 n*M*, while we test the sensitivity of deep water Fe_T to the value of L_T. Here, dissolved iron is assumed to be the sum of "free" and "complexed" forms,

$$Fe_T = Fe' + FeL. \quad (12)$$

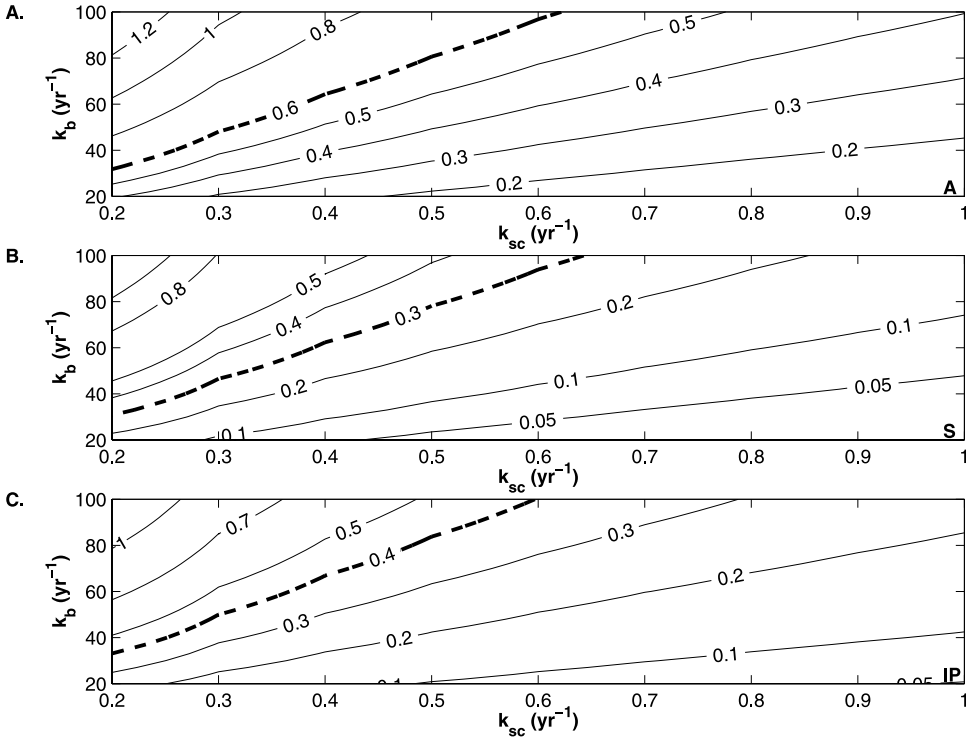

Figure 5. Scavenging-desorption model: Sensitivity of deep [Fe_T] to scavenging/desorption rate constants. [Fe_T] as a function of scavenging (k_{sc}, yr^{-1}) and desorption (k_b, yr^{-1}) for (a) Atlantic, (b) Southern Ocean, and (c) Indo-Pacific basin. The dashed contours indicate the average observed [Fe_T] for each basin. The optimal solution is for $k_b/k_{sc} \sim 150-170$.

Here *FeL* represents the complexed iron associated with an organic ligand. Only the free form is available for scavenging and hence,

$$J_{Fe} = -k_{sc} Fe'. \tag{13}$$

Since complexation occurs on very rapid timescales, it is assumed that the reaction goes to equilibrium. We specify the total ligand concentration, $L_T = [FeL] + [L']$, and use the equilibrium relationship $K_{FeL}^{cond} = [FeL]/[Fe'][L']$ to determine the speciation of the iron. Fe_T is a conservative property with respect to transport. Desorption from particles is neglected in this case since its impact is overwhelmed by the strong complexation reaction.

[37] Setting L_T to 1 n*M*, in Figure 7 we plot the relationship of the deep water dissolved iron concentration in each basin to scavenging rate, ranging between 0.2 and 1.8 yr^{-1} and conditional stability constant, K_{FeL}, between $10^{10} M^{-1}$ and $10^{13} M^{-1}$, reflecting the range of values inferred from ocean observations [*Gledhill and van den Berg*, 1994; *Rue and Bruland*, 1995; *van den Berg*, 1995; *Wu and Luther*, 1995; *Rue and Bruland*, 1997; *Gledhill et al.*, 1998; *Nolting et al.*, 1998; *Witter and Luther*, 1998; *Witter et al.*, 2000; *Boye et al.*, 2001; *Powell and Donat*, 2001]. Since K_{FeL} and deep water [Fe] are constrained by measurements, this sensitivity study can also constrain the scavenging rate of Fe, although it has not been measured. Deep iron concentrations generally increase with increasing stability constant

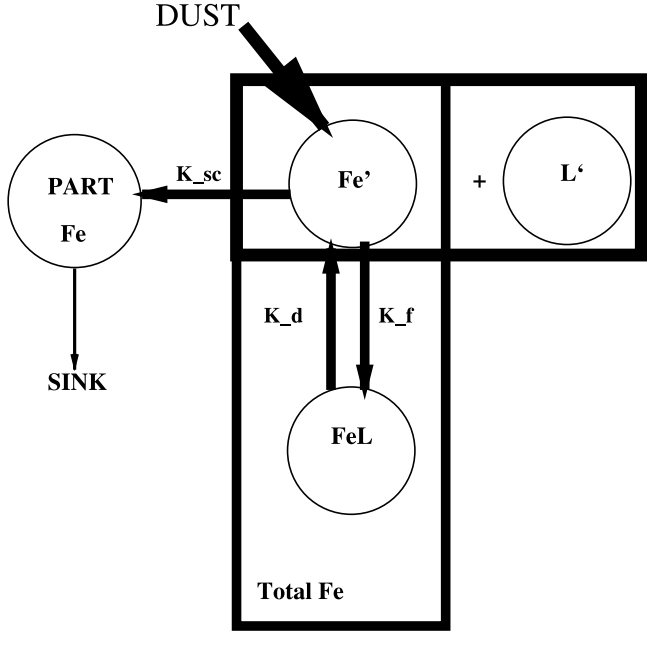

Figure 6. Schematic diagram of the complexation model. Dissolved Fe can undergo two transformations: It can be scavenged or it can be complexed. The box represents the reaction Fe′ + L′ = FeL. We assume that chemical forms within the box (Fe′ and FeL) can be utilized biologically, but only Fe′ can be scavenged.

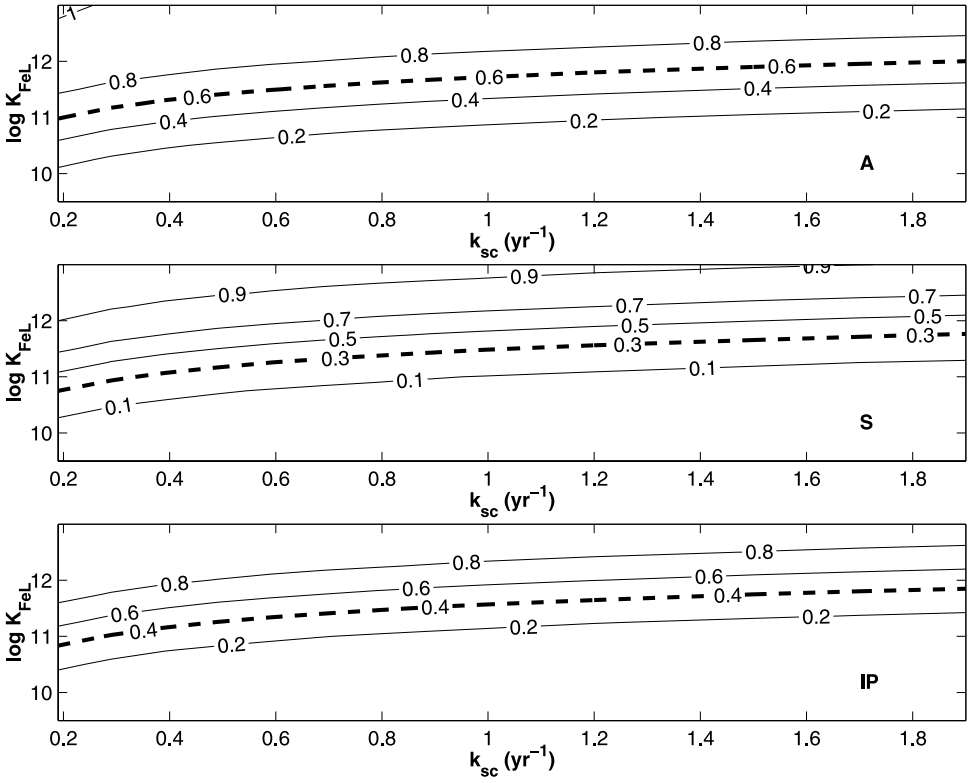

Figure 7. Complexation model: Sensitivity of [Fe_T] to scavenging (k_{sc}, yr^{-1}) and conditional stability constant (log $K_{Fe'L}$) for the (a) Atlantic, (b) Southern Ocean, and (c) Indo-Pacific basin with [L_T] = 1 n*M*. The dashed contour represents the average observed deep water [Fe] for each basin.

and decreasing scavenging rate. Since only the uncomplexed form of iron can be scavenged, at high scavenging rates a strong ligand is required to maintain deep water "dissolved" [Fe_T] concentrations at observed levels, sequestering it in a form which we assume is not available for scavenging. At very low scavenging rates, the sensitivity to the conditional stability constant decreases, since it is no longer necessary for iron to be in complexed form to remain in the water column for a significant period. The sensitivity to the scavenging constant is weak when scavenging is strong because there is very little scavengable iron and the limiting process is complexation.

[38] Observations indicate that while most "dissolved" iron is in complexed form, a significant fraction of ligand is free [*Gledhill and van den Berg*, 1994; *Rue and Bruland*, 1995; *van den Berg*, 1995; *Wu and Luther*, 1995; *Rue and Bruland*, 1997; *Gledhill et al.*, 1998; *Nolting et al.*, 1998; *Witter and Luther*, 1998; *Witter et al.*, 2000; *Boye et al.*, 2001; *Powell and Donat*, 2001]. This is in contrast to the models of *Archer and Johnson* [2000] and *Lefévre and Watson* [1999] where, due to the low total ligand concentration and high conditional stability constant, the dissolved iron concentration was about the same as the total ligand concentration (0.6 n*M*) over much of the ocean. This case, where the ligand is saturated, represents a limit case of the scheme used here. By relaxing these constraints, it is possible to find a solution consistent with the observed iron distribution which also predicts a significant presence of free ligand, L'. Figure 8 shows the dependency of [L'] on K_{FeL} and scavenging rate constant for this model with specified total ligand concentration of 1 n*M*. As the scavenging rate increases, the loss of Fe limits the complexation reaction, resulting in excess free ligand, [L']. Comparing Figure 7 and Figure 8, Fe_T and L are inversely related. For strong K_{FeL}, $Fe_T \approx FeL$, which is the limit modeled by *Archer and Johnson* [2000] and implicitly by *Lefévre and Watson* [1999].

[39] Observations also indicate a significant variation in ligand concentration around the ocean but, as yet, without a clearly emerging large-scale pattern [*Gledhill and van den Berg*, 1994; *Rue and Bruland*, 1995; *van den Berg*, 1995; *Wu and Luther*, 1995; *Rue and Bruland*, 1997; *Gledhill et al.*, 1998; *Nolting et al.*, 1998; *Witter and Luther*, 1998; *Witter et al.*, 2000; *Boye et al.*, 2001; *Powell and Donat*, 2001]. Still without introducing any spatial variations in the ligand concentration, we also illustrate the sensitivity of dissolved iron and free ligand concentrations to the concentration of total ligand. Figures 9 and 10 show the deep ocean iron concentration and free ligand concentration, respectively, (as Figures 7 and 8), but with increased total ligand concentration, L_T = 4 n*M*. For identical choices of k_{sc} and K_{FeL} with increased total ligand, we find increased [Fe_T]. Hence, to fit the modern observed distribution with L_T = 4 n*M*, we must adjust k_{sc} by a factor of $\sim$15–25 times. However, the sensitivity pattern is the same.

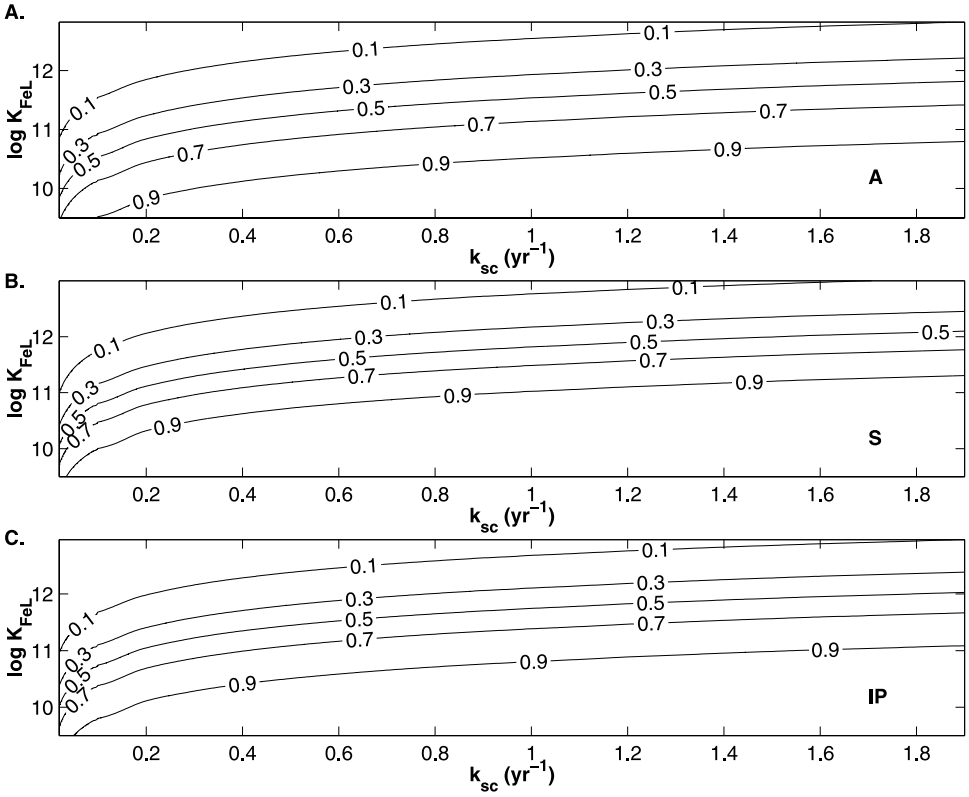

Figure 8. Complexation model: Sensitivity of the free ligand concentration ([L′]) to scavenging rate (k_{sc}, yr^{-1}) and conditional stability constant ($\log K_{Fe'L}$) for the (a) Atlantic, (b) Southern Ocean, and (c) Indo-Pacific basin with $[L_T] = 1$ n*M*. As $\log K_{Fe'L}$ increases, [L] decreases due to forward reaction $L' + Fe' = FeL$. As scavenging increases, [L] increases, as forward reaction is limited by Fe, resulting in excess L.

[40] The model predicts an excess [L′] ranging from 0.5 to 3 n*M* for scavenging rates between 0.2 and 1.8 yr^{-1} and ligand strengths ranging from $\log(K_{FeL})$ of 10 to 13 (Figure 10). It suggests highest excess [L′] for the Atlantic basin, in broad agreement with observations [*Gledhill and van den Berg*, 1994; *Rue and Bruland*, 1995; *van den Berg*, 1995; *Wu and Luther*, 1995; *Rue and Bruland*, 1997; *Gledhill et al.*, 1998; *Nolting et al.*, 1998; *Witter and Luther*, 1998; *Witter et al.*, 2000; *Boye et al.*, 2001; *Powell and Donat*, 2001].

4. Discussion

[41] We have examined three parameterizations of water column iron biogeochemistry in the framework of an idealized, six-box ocean biogeochemistry model. In the light of the latest available observations of the deep ocean distribution of iron, an extremely simple model which parameterizes deep ocean biogeochemical cycling of iron as a first-order net scavenging is able to capture the broad basin to basin structures for residence times, with respect to scavenging, of a hundred years or so. However, this parameterization does not explicitly represent the processes believed to control the system. A second parameterization treated iron as an analogue of thorium, with rapid scavenging and desorption of iron to and from particles. For a scavenging/desorption rate constant of ~150, this model can also reproduce the broad features of the large-scale distribution of dissolved iron.

[42] In a third parameterization, following *Archer and Johnson* [2000], we introduce complexation to an organic ligand. Sensitivity studies showed that this model can reproduce the large-scale iron distribution over the range of ligand strengths observed (K_{FeL}) and also constrains the scavenging rate (k_{sc}) for a range of total ligand concentrations, L_T. The ligand parameterization of *Leféyre and Watson* [1999] and *Archer and Johnson*'s [2000] complexation with one ligand case, with a very strong ligand and low total ligand concentration, both led to quite uniform deep ocean iron distributions and saturated ligand. This is a limit case of the more general model presented here. The model and recent observational data suggest that the parameter choices of *Archer and Johnson*'s [2000] two-ligand model, with a very strong ligand in the upper ocean resulting in fairly uniform deep water [Fe_T], is at odds with recent observational evidence. It would also lead to high iron and low phosphorus concentrations at the surface. To prevent the accumulation of iron in surface waters, *Archer and Johnson* [2000] remove any surface iron from the system that is not utilized biologically, but the process this should represent is not clearly identified. On the basis of the sensitivity studies performed here and recent observational data, we suggest that a parameter regime with a weaker ligand and greater concentration of total ligand may be more

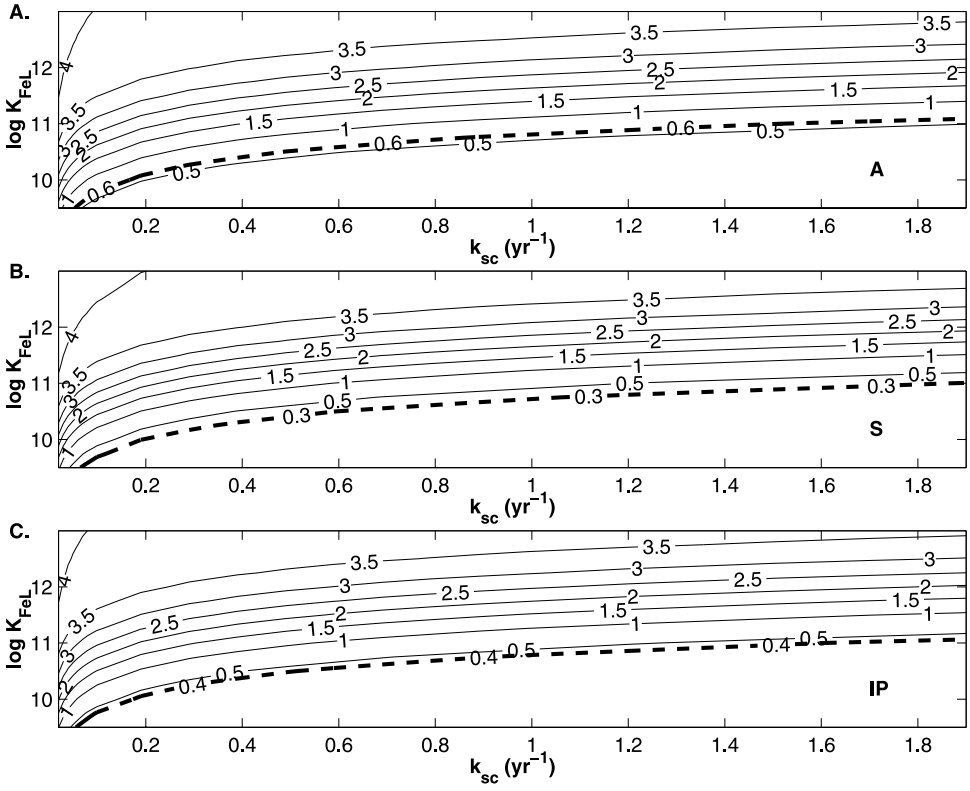

Figure 9. Complexation model: Sensitivity of modeled deep water [Fe_T] to scavenging rate (k_{sc}, yr^{-1}) and conditional stability constant (log $K_{Fe'}L$) for the (a) Atlantic, (b) Southern Ocean, and (c) Indo-Pacific basin with [L_T] = 4 nM. The dashed contour represents the observed average deep water [Fe_T] for each basin.

realistic. In the latter case, the model can reproduce both the deep iron distribution and also the observed presence of significant amounts of free ligand.

5. Sensitivity to Aeolian Iron Source

[43] A strong motivation for developing such parameterizations is to be able to explicitly describe and explore the role of iron in setting current, past, and future ocean distributions of carbon and macronutrients. Of particular interest is the possible impact and feedbacks of climate change and the aeolian supply of iron to the remote Southern Ocean. *Martin* [1990] suggested increased dust flux during the Last Glacial Maximum (LGM) could have increased export production and decreased atmospheric pCO_2 in the Southern Ocean. While data from ice cores [*Petit et al.*, 1999] and models [*Mahowald et al.*, 1999] suggest that the global dust flux increased 2–5 times relative to present-day, paleo productivity proxies do not suggest that export production was higher during the Last Glacial Maximum (LGM) in the Southern Ocean [*Francois et al.*, 1997; *Kumar et al.*, 1995]. Rather, $\delta^{15}N$ data suggests increased efficiency of nutrient utilization in the high latitudes, perhaps due to weaker vertical exchange [*Francois et al.*, 1997].

[44] Here we explore the sensitivity of the iron biogeochemistry parameterizations to the magnitude of the global aeolian iron supply and the strength of vertical exchange between the Southern Ocean surface and deep waters. Each parameterization was able to reproduce the broad features of the known modern distribution provided that certain free parameter values could be assumed.

[45] In Figure 11, for each parameterization, we plot the Southern Ocean surface [PO_4] as a function of a global increase in aeolian iron supply, relative to today's, and for several rates of Southern Ocean vertical mass exchange. By increasing the dust flux 10 times globally, surface [PO_4] is depleted in both the net scavenging and scavenging/desorption models (Figures 11a and 11b). There is little sensitivity to the strength of Southern Ocean overturning. In strong contrast, for the complexation parameterization (Figure 11c), even with global dust increase of 10 times and the strength of vertical exchange decreased by 50%, it is not possible to completely drawdown surface [PO_4] in this model.

[46] The importance of Fe supplied to the euphotic zone by dust compared to upwelled Fe gives insight into the underlying mechanistic differences. We plot the fraction of iron supplied by dust to the surface Southern Ocean (Figure 12) and the deep water dissolved iron concentration (Figure 13) for the three models. In each case, upwelling is the dominant source of iron to the euphotic zone under conditions of modern dust deposition, in agreement with the findings of *Fung et al.* [2000]. The models respond differently as global dust flux increases. For the net scavenging and scavenging/

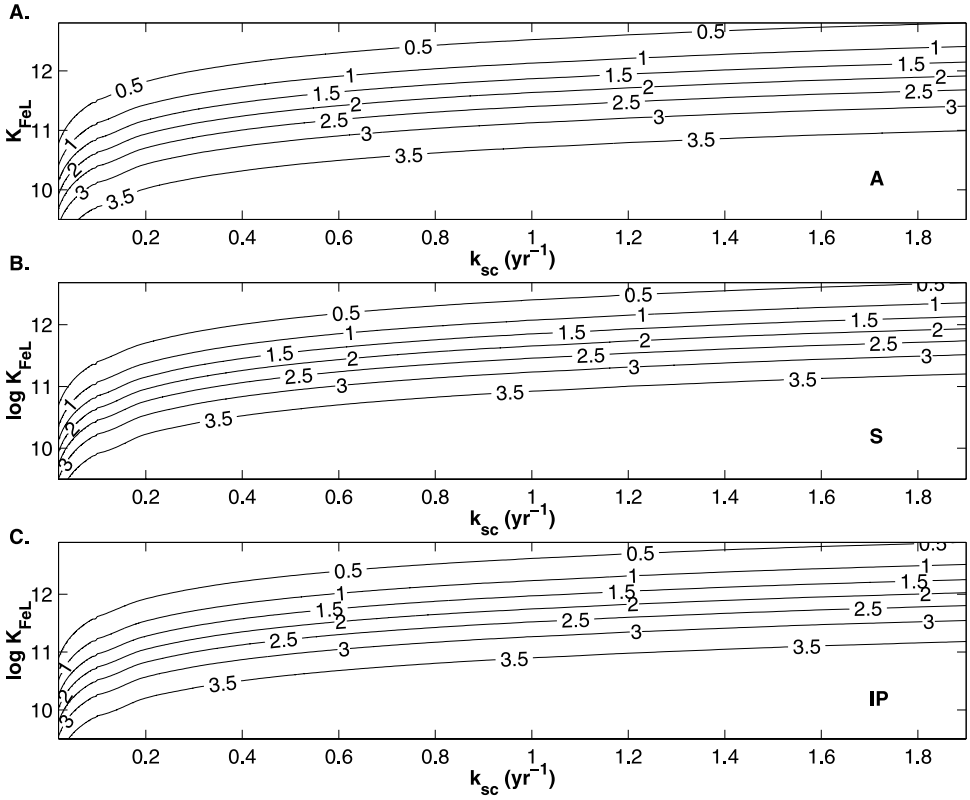

Figure 10. Complexation model: Same as Figure 8, but $[L_T]$ = 4 n*M*.

desorption parameterization, the fraction of iron supplied regionally by dust is small (5–10%), and insensitive to the global aeolian dust supply (Figures 12a and 12b). This is because the slow net scavenging rate enables iron derived from low-latitude dust to be transported at depth to the deep Southern Ocean. Therefore the upwelled source of iron from the Southern Ocean increases in proportion to the global dust deposition (Figures 13a and 13b). For the complexation parameterization, the fraction of iron supplied by dust increases strongly with aeolian dust deposition (Figure 12c). This is because the imposed, finite ligand concentration places an upper limit on the deep water iron concentration (Figure 13c) and therefore on the upwelled iron source. It is possible that ligand production increases as a function of increased dust flux, as evidenced by *Rue and Bruland* [1997] during the Iron-Ex II study in the equatorial Pacific. As our sensitivity study using the complexation model with an elevated $[L_T]$ = 4 n*M* shows, deep water $[Fe_T]$ would increase with increasing total ligand concentration, and so might the upwelling supply. However, we have not parameterized this specific mechanism here.

[47] Three different parameterizations of deep water iron cycling are able to capture the observed distribution of iron in the modern ocean. The complexation parameterization apparently resolves more details of the system as it is presently understood. However, these parameterizations lead to very different sensitivities of surface phosphate drawdown in conditions of increased dust supply. It is premature to suggest that one parameterization is more realistic than another in this regard, but it is very significant for model projections of glacial-interglacial biogeochemical change, such as that of *Watson et al.* [2000], which applied a scavenging based parameterization. Clearly, it is imperative to continue to seek more observational data and a deeper understanding of the key processes in order to make more appropriate models for climate change studies.

6. Summary and Outlook

[48] We have examined several parameterizations of iron biogeochemistry in the context of an idealized, six-box ocean biogeochemistry model. Imposing present-day estimates of the aeolian iron supply and its regional variations, we show that each of the three models may be made to fit the broad, basin to basin, distribution of "dissolved" iron in the oceans deep waters, as it is currently known, provided that certain parameter values can be assumed. For the simplest model representing a net scavenging of iron from the water column, and not attempting to explicitly represent the detailed processes, if the lifetime of dissolved iron with respect to scavenging is of the order of 100 years, the model is broadly consistent with the observed data. A more detailed model, including rapid scavenging and complexation with an organic ligand, of uniform total concentration can also fit the data over a range of parameter values which fall within the observed oceanic ranges. Previously published models with a similar basis (*Lefèvre and Watson* [1999] and *Archer and Johnson* [2000], single ligand case) have represented the limit where the total ligand concentration is low, and the ligand very strong, leading to uniform

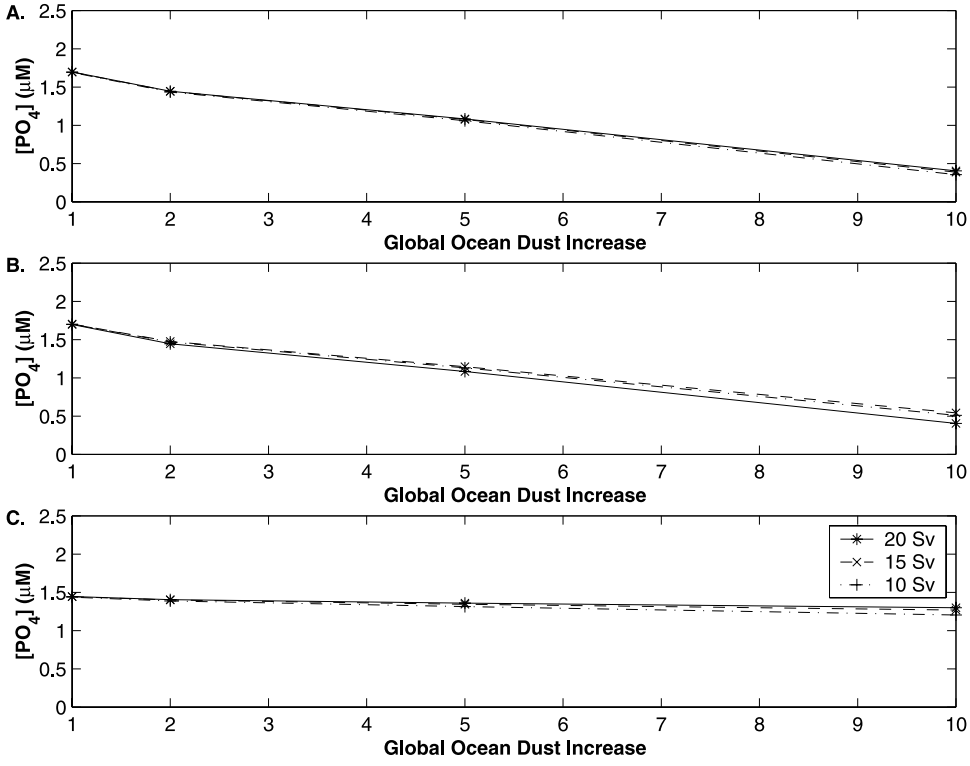

Figure 11. Steady state surface Southern Ocean PO_4 sensitivity to global dust increase and Southern Ocean overturning (Sv) for (a) net scavenging case, (b) scavenging/desorption case, and (c) complexation case. For the net scavenging and scavenging/desorption case, an increase in global dust supply results in the drawdown of PO_4 with little sensitivity to the strength of vertical exchange. For the complexation case (Figure 11c), PO_4 drawdown is muted.

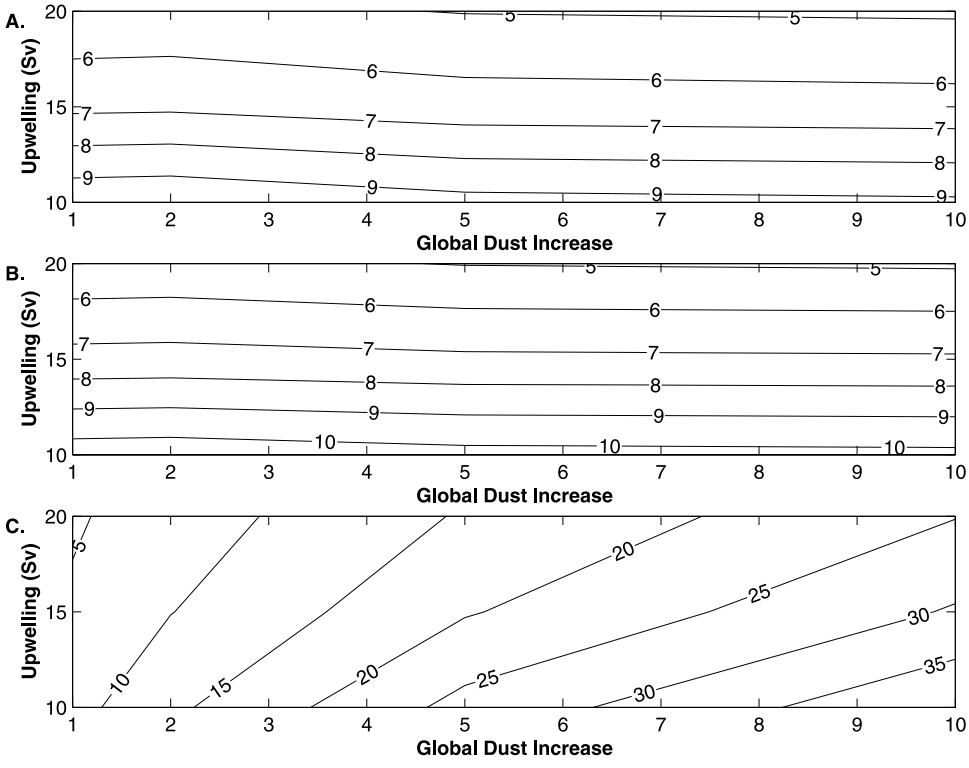

Figure 12. Percent iron in surface Southern Ocean derived from dust (dust/dust + upwelling) for the (a) net scavenging case, (b) scavenging and desorption case, and (c) complexation case as a function of dust flux and Southern Ocean overturning.

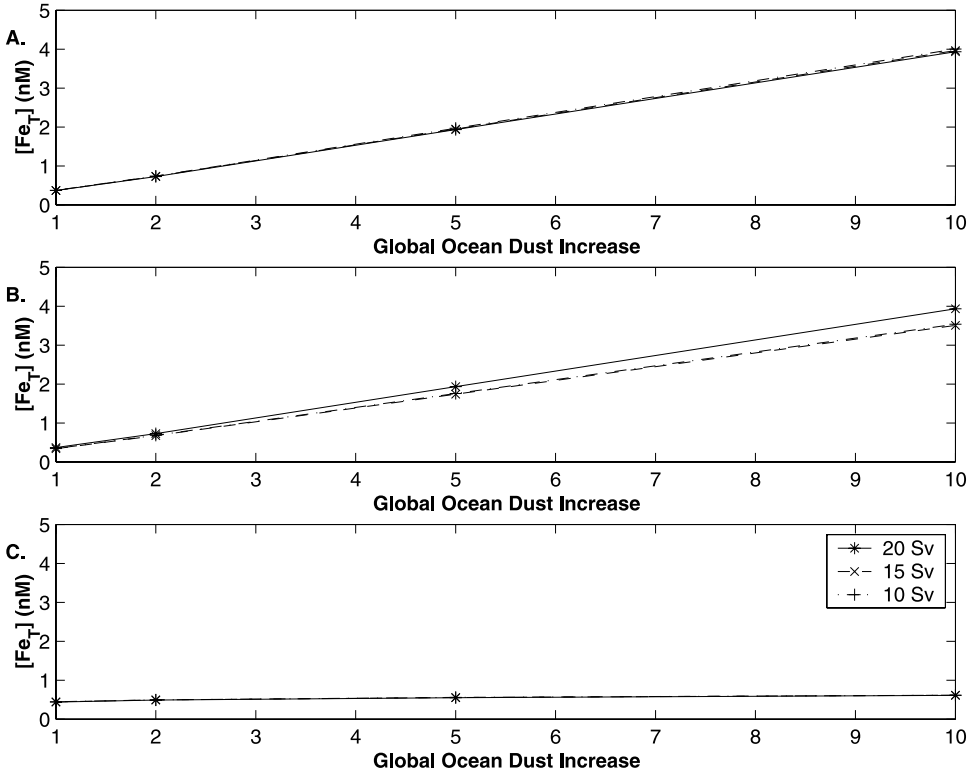

Figure 13. Southern Ocean deep Fe_T response to global ocean dust increase and upwelling strength for (a) net scavenging case, (b) scavenging/desorption case, and (c) complexation case. For the net scavenging and scavenging/desorption case, an increase in global dust supply results in a proportional increase in deep water [Fe_T]. For the complexation case (Figure 13c), Southern Ocean deep water [Fe_T] increase is much less than in Figures 13a and 13b.

concentrations of iron in the deep ocean and implying that the ligand is saturated. We argue, based on this model, that a weaker ligand and greater total ligand concentration are more appropriate choices. In addition to reproducing the broad patterns of ocean iron, this choice also predicts significant amounts of free ligand, consistent with recent observational studies.

[49] We have explored the sensitivity of the surface phosphate concentration in the Southern Ocean to the aeolian iron supply for each of these parameterizations. We find a strong contrast between the scavenging-based models, in which the deep iron concentration and upwelling iron supply to the surface Southern Ocean increase in concert with enhanced aeolian supply. In these models, surface phosphate can be completely drawn down. On the other hand, in the case where deep iron concentrations are controlled by complexation with an organic ligand, the drawdown of phosphate asymptotes toward a non-zero value which reflects the upper limit of deep dissolved iron imposed by the available ligand. Hence, in this case, the potential for drawdown of surface phosphate relative to the modern ocean depends on the current availability of free ligand and the possibility of increased ligand production in response to an increased dust flux.

[50] Such highly idealized models are very efficient tools for exploring several parameterizations over a wide range of parameter space. However, such simplified models may be quantitatively misleading [e.g., *Archer et al.*, 2000], and one should view the results as such. However, these models have revealed significant qualitative differences in the sensitivity of these parameterizations to increasing dust supply. This should also be examined in the context of more complex, global, three-dimensional, biogeochemical models. This is the focus of an ongoing study.

[51] We suggest that this model has demonstrated the capabilities and sensitivities of current iron parameterizations. However, these are still very simplistic, in part constrained by the present lack of observational data due to the difficulty of making appropriate measurements. We strongly encourage efforts that will lead to a more complete global survey of the distribution of iron in the oceans and better quantification, characterization, and understanding of the organic ligands which seem to play such an important role. Advances in modeling and interpretation of the sensitivity of the system to global change will only be enabled through the availability of such data.

[52] **Acknowledgments.** M. J. F. is grateful for funding from NOAA (NA16GP2988) and NSSF (OCE-336839). P. P. is grateful to the MIT Martin Fellowship and NASA Earth System Science Fellowship (NGT5-30362) for funding.

References

Archer, D., and K. Johnson (2000), A model of the iron cycle in the ocean, *Global Biogeochem. Cycles*, *14*, 269–279.

Archer, D., G. Eshel, A. Winguth, W. Broecker, R. Pierrehumbert, M. Tobis, and R. Jacob (2000), Atmospheric pCO_2 sensitivity to the biological pump of the ocean, *Global Biogeochem. Cycles*, *14*, 1219–1230.

Bacon, M., and R. Anderson (1982), Distribution of thorium isotopes between dissolved and particulate forms in the deep sea, *J. Geophys. Res.*, *87*, 2045–2056.

Bell, J., J. Betts, and E. Boyle (2002), MITESS: A moored in situ trace element serial sampler for deep sea moorings, *Deep Sea Res., Part I*, *49*, 2108–2118.

Boyd, P., et al. (2000), A mesoscale phytoplankton bloom in the polar Southern Ocean stimulated by iron fertilization, *Nature*, *407*, 695–702.

Boye, M., C. van den Berg, J. de Jong, H. Leach, P. Croot, and H. de Baar (2001), Organic complexation of iron in the Southern Ocean, *Deep Sea Res., Part I*, *48*, 1477–1497.

Boyle, E. (1997), What controls dissolved iron concentrations in the world ocean?—A comment, *Mar. Chem.*, *57*, 163–167.

Broecker, W., and T. Peng (1986), Carbon cycle: 1985 glacial to interglacial changes in the operation of the global carbon cycle, *Radiocarbon*, *28*, 309–327.

Broecker, W., and T. Peng (1987), The role of $CaCO_3$ compensation in the glacial to interglacial atmospheric CO_2 change, *Global Biogeochem. Cycles*, *1*, 15–29.

Broecker, W., J. Lynch-Stieglitz, D. Archer, M. Hoffmann, E. Maier-Reimer, O. Marchal, T. Stocker, and N. Gruber (1999), How strong is the Harvdton-Bear constraint?, *Global Biogeochem. Cycles*, *13*, 817–820.

Bruland, K. W., K. J. Orians, and J. P. Cowen (1994), Reactive trace metals in the stratified central North Pacific, *Geochem. Cosmochim. Acta*, *58*, 3171–3182.

Coale, K., S. Fitzwater, R. Gordon, K. Johnson, and R. Barber (1996), Control of community growth and export production by upwelled iron in the equatorial Pacific Ocean, *Nature*, *379*, 621–624.

Cochran, J., K. Buesseler, M. Bacon, and H. Livingston (1993), Thorium isotopes as indicators of particle dynamics in the upper ocean: Results from the JGOFS North Atlantic Bloom Experiment, *Deep Sea Res., Part I*, *40*, 1569–1595.

Conkright, M. E., H. E. Garcia, T. D. O'Brien, R. A. Locarnini, T. P. Boyer, C. Stephens, and J. I. Antonov (2002), *World Ocean Atlas 2001*, vol. 4, *Nutrients*, edited by S. Levitus, *NOAA Atlas NESDIS 52*, Natl. Oceanic and Atmos. Admin., Silver Spring, Md.

de Baar, H. J., J. T. de Jong, R. F. Nolting, K. R. Timmermans, M. A. van Leeuwe, U. Bathmann, M. R. van der Loeff, and J. Sildam (1999), Low dissolved Fe and the absence of diatom blooms in remote Pacific waters of the Southern Ocean, *Mar. Chem.*, *66*, 1–34.

Duce, R., and N. Tindale (1991), Atmospheric transport of iron and its deposition in the ocean, *Limnol. Oceanogr.*, *36*, 1715–1726.

Fitzwater, S., K. Coale, R. Gordon, K. Johnson, and M. Ondrusek (1996), Iron deficiency and phytoplankton growth in the equatorial Pacific, *Deep sea Res., Part II*, *43*, 995–1015.

Follows, M., T. Ito, and J. Marotzke (2002), The wind-driven subtropical gyres and atmospheric pCO_2, *Global Biogeochem. Cycles*, *16*(4), 1113, doi:10.1029/2001GB001786.

Francois, R., M. Altabet, E. Yu, D. Sigman, M. Bacon, M. Frank, G. Bohrmann, G. Bareille, and L. Labeyrie (1997), Contribution of Southern Ocean surface-water stratification to low atmospheric CO_2 concentrations during the last glacial period, *Nature*, *389*, 929–935.

Fung, I., S. Meyn, I. Tegen, S. Doney, J. John, and J. Bishop (2000), Iron supply and fixation in the upper ocean, *Global Biogeochem. Cycles*, *14*, 281–295.

Gao, Y., Y. Kaufman, D. Tanre, D. Kolber, and P. Falkowski (2001), Seasonal distribution of aeolian iron fluxes to the global ocean, *Geophys. Res. Lett.*, *28*, 29–32.

Gledhill, M., and C. van den Berg (1994), Determination of complexation of iron (III) with natural organic complexing ligands in seawater using cathodic stripping voltammetry, *Mar. Chem.*, *47*, 41–54.

Gledhill, M., C. van den Berg, R. Nolting, and K. Timmermans (1998), Variability in the speciation of iron in the northern North Sea, *Mar. Chem.*, *59*, 283–300.

Jickells, T., and L. Spokes (2002), Atmospheric iron inputs to the oceans, in *The Biogeochemistry of Iron in Seawater*, edited by D. R. Turner and K. A. Hunter, pp. 85–121, John Wiley, New York.

Johnson, K., R. Gordon, and K. Coale (1997), What controls dissolved iron concentrations in the world ocean?, *Mar. Chem.*, *57*, 137–161.

Kumar, N., R. Anderson, R. Mortlock, P. Froelich, P. Kubik, B. Dittrich-Hannen, and M. Suter (1995), Increased biological productivity and export production in the glacial Southern Ocean, *Nature*, *378*, 675–680.

Lefévre, N., and A. J. Watson (1999), Modeling the geochemical cycle of iron in the oceans and its impact on atmospheric CO_2 concentrations, *Global Biogeochem. Cycles*, *13*, 727–736.

Macrellis, H., C. Trick, E. Rue, G. Smith, and K. Bruland (2001), Collection and detection of natural iron-binding ligands from seawater, *Mar. Chem.*, *76*, 175–187.

Mahowald, N., K. Kohfeld, M. Hansson, Y. Balkanski, S. Harrison, I. Prentice, M. Schulz, and H. Rodhe (1999), Dust sources and deposition during the Last Glacial Maximum and current climate: A comparison of model results with paleodata from ice cores and marine sediments, *J. Geophys. Res.*, *104*, 15,895–15,916.

Martin, J. (1990), Glacial-interglacial CO_2 change: The iron hypothesis, *Paleogeography*, *5*, 1–13.

Martin, J., et al. (1994), Testing the iron hypothesis in ecosystems of the equatorial Pacific Ocean, *Nature*, *371*, 123–129.

Nolting, R., L. Gerringa, M. Swagerman, K. Timmermans, and H. de Baar (1998), Fe (III) speciation in the high nutrient, low chlorophyll Pacific region of the Southern Ocean, *Mar. Chem.*, *62*, 335–352.

Petit, J., et al. (1999), Climate and atmospheric history of the past 420,000 years from the Vostok ice core, Antarctica, *Nature*, *399*, 429–436.

Powell, R., and J. Donat (2001), Organic complexation and speciation of iron in the South and Equatorial Atlantic, *Deep Sea Res., Part II*, *48*, 2877–2893.

Price, N., L. Anderson, and F. Morel (1994), The equatorial Pacific Ocean: Grazer-controlled phytoplankton populations in an iron-limited ecosystem, *Limnol. Oceanogr.*, *39*, 520–534.

Rue, E., and K. Bruland (1995), Complexation of iron(III) by natural organic ligands in the central North Pacific as determined by a new competitive ligand equilibration/adsorptive cathodic stripping voltammetric method, *Mar. Chem.*, *50*, 117–138.

Rue, E., and K. Bruland (1997), The role of organic complexation on ambient iron chemistry in the equatorial Pacific Ocean and the response of a mesoscale iron addition experiment, *Limnol. Oceanogr.*, *42*, 901–910.

Sarmiento, J., and J. Orr (1991), Three-dimensional simulations of the impact of Southern Ocean nutrient depletion on atmospheric CO_2 and ocean chemistry, *Limnol. Oceanogr.*, *36*, 1928–1950.

Sohrin, Y., S. Iwamoto, M. Matsui, H. Obata, E. Nakayama, K. Suzuki, N. Handa, and M. Ishii (2000), The distribution of Fe in the Australian sector of the Southern Ocean, *Deep Sea Res., Part I*, *47*, 55–84.

Spokes, L., and T. Jickells (1996), Factors controlling the solubility of aerosol trace metals in the atmosphere and on mixing into seawater, *Aquat. Geochem.*, *1*, 355–374.

Sunda, W., and S. Huntsman (1995), Iron uptake and growth limitation in oceanic and coastal phytoplankton, *Mar. Chem.*, *50*, 189–206.

van den Berg, C. (1995), Evidence for organic complexation of iron in seawater, *Mar. Chem.*, *50*, 139–157.

Watson, A., D. Bakker, A. Ridgwell, P. Boyd, and C. Law (2000), Effect of iron supply on Southern Ocean CO_2 uptake and implications for glacial atmospheric CO_2, *Nature*, *407*, 730–733.

Witter, A., and G. Luther (1998), Variation in Fe(III)-organic complexation with depth in the northwestern Atlantic Ocean as determined using a kinetic approach, *Mar. Chem.*, *62*, 241–248.

Witter, A., D. Hitchins, A. Butler, and G. Luther (2000), Determination of conditional stability constants and kinetic constants for strong model Fe-binding ligands in seawater, *Mar. Chem.*, *69*, 1–17.

Wu, J., and E. Boyle (2002), Iron in the Sargasso Sea: Implications for the processes controlling dissolved Fe distribution in the ocean, *Global Biogeochem. Cycles*, *16*(4), 1086, doi:10.1029/2001GB001453.

Wu, J., and G. Lutler (1994), Size-fractionate iron concentrations in the water column of the North Atlantic Ocean, *Limnol. Oceanogr.*, *39*, 1119–1129.

Wu, J., and G. Luther (1995), Complexation of Fe(III) by natural organic ligands in the Northwest Atlantic Ocean by a competitive ligand equilibration method and kinetic approach, *Mar. Chem.*, *50*, 159–177.

Wu, J., E. Boyle, W. Sunda, and L. Wen (2001), Soluble and colloidal iron in the oligotrophic North Atlantic and North Pacific, *Science*, *293*, 847–849.

Yamanaka, Y., and E. Tajika (1997), Role of dissolved organic matter in the marine biogeochemical cycles: Studies using an ocean biogeochemical general circulation-model, *Global Biogeochem. Cycles*, *11*, 599–612.

E. Boyle, M. J. Follows, and P. Parekh, Department of Earth, Atmospheric and Planetary Sciences, Massachusetts Institute of Technology, 77 Massachusetts Avenue, Cambridge, MA 02139, USA. (pparekh@mit.edu)

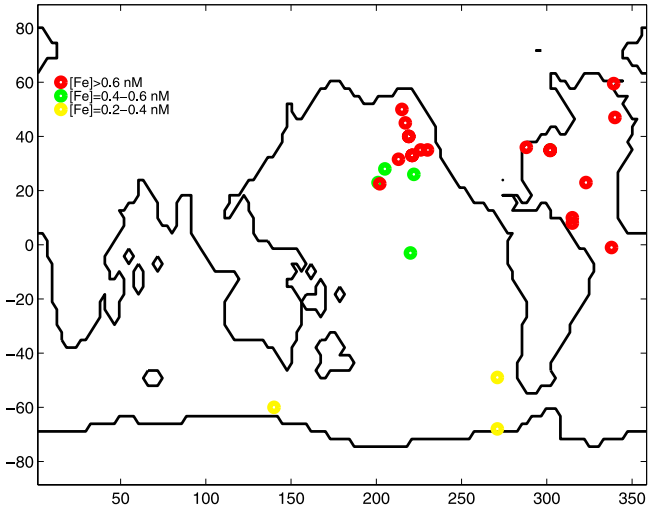

Figure 1. Observed dissolved [Fe] (<0.4 μm) at 1000 m. Data sources: *Bell et al.* [2002], E. Boyle (unpublished data), *Bruland et al.* [1994], *de Baar et al.* [1999], *Johnson et al.* [1997, and references therein], *Powell and Donat* [2001], *Rue and Bruland* [1995], *Sohrin et al.* [2000], *Wu and Luther* [1994], *Wu et al.* [2001], and *Wu and Boyle* [2002].